Localized topological states in Bragg multihelicoidal fibers with twist defects

C. N. Alexeyev,[1,*] B. P. Lapin,[1] G. Milione,[2] and M. A. Yavorsky[1]

[1]*V. I. Vernadsky Crimean Federal University, Vernadsky Prospekt, 4, Simferopol 295007, Crimea, Ukraine*

[2]*Institute for Ultrafast Spectroscopy and Lasers, Physics Department, City College of New York of the City University of New York, 160 Convent Avenue, New York, New York 10031, USA*

(Received 29 March 2016; published 16 June 2016)

We have studied the influence of a twist defect in multihelicoidal Bragg fibers on the emerging of localized defect modes. We have shown that if such a fiber is excited with a Gaussian beam this leads to the appearance of a defect-localized topological state, whose topological charge coincides with the order of rotational symmetry of the fiber's refractive index. We have shown that this effect has a pronounced crossover behavior. We have also formulated a principle of creating the systems that can nestle defect-localized topologically charged modes. According to this principle, such systems have to possess topological activity, that is, the ability to change the topological charge of the incoming field, and operate in the Bragg regime.

DOI: 10.1103/PhysRevA.93.063829

I. INTRODUCTION

Since the discovery of Anderson localization—the absence of diffusion of electrons in disordered lattices—the constructive role of static defects in the creation of localized states has been recognized [1,2]. Subsequently, it has been found that localized states can form not only in the presence of randomly positioned defects, but also on single defects in periodic dielectric structures. The idea to use regular defects in such structures dates back to the seminal papers by Yablonovitch [3,4]. Introducing defects in photonic band-gap structures enables creation of low-loss waveguides in them [5]. As has been pointed out [4], for band-gap photonic structures the presence of a localized defect results in the emergence of a localized defect mode, the spectral line of which is positioned within the forbidden spectral band. It is the existence of such defect-localized gap mode that enables low-threshold lasing through this frequency window created by the defect mode while spontaneous emission occurs in solids. This property has found application in vertical cavity surface-emitting lasers, in which an amplifying defect layer is sandwiched between periodic dielectric structures [6]. Also photonic band-gap structures with defects may be used for narrow-band filters [7] and for second harmonic emission due to an enhancement of nonlinear phenomena at defects [8].

The type of a defect which can be created in a periodic structure essentially depends on the symmetry of the dielectric lattice. In this way, for a layered structure, which is the most common representation of a one-dimensional (1D) photonic crystal, such a localized defect can be implemented by changing the width of the particular layer or its refractive index. Unlike photonic crystals composed of isotropic materials, the band-gap anisotropic structures allow greater versatility in defects insertion. One of the most important types of such systems is a periodic chiral medium, an example of which is given by self-organized cholesteric liquid crystals. Such systems allow an additional degree of freedom in inserting the defect, namely, twisting one part of the sample with respect to the other chiral structure. This type of a defect can be experimentally created by glancing-angle deposition on a rotating substrate [5]. For a millimeter-wavelength range such chiral media with a twist defect can be made of stacks of transparency sheets [9,10]. In the optical range such a twist defect was demonstrated for cholesteric polymer films [11,12]. Transmission characteristics of such a 1D chiral crystal with a twist defect were shown to demonstrate a pronounced crossover behavior, which had been attributed to the presence of a localized mode, nested on the defect.

Despite essential progress achieved in this area, those studies were limited to the case of the waves with no wave-front dislocations. Recent progress in singular optics [13] has opened new possibilities for investigations of the evolution of topologically charged electromagnetic waves in optical media with defects. The questions of Anderson localization for the light with topological dislocations in waveguides are currently under consideration [14]. In this paper we make a further step in studying defect-localized modes with embedded topological charge. Leaving beyond its scope the matters concerned with localization in the presence of random defects, we focus our attention on studying the periodic chiral structure with a single defect of a twist discontinuity type.

Simple geometry of transversely homogeneous layered media does not allow imprinting any topological charge into the structure. This can be achieved only in optical systems with specially engineered transverse distribution of the refractive index. As has been recently shown, such imprinting of the topological charge can be attained in multihelicoidal fibers (MHFs) [15], in which refractive index distribution forms l spirals (l is an integer). As has been demonstrated, at certain conditions MHFs change the topological charge of the incoming beam by $\pm l$. Such systems with multifold symmetry of the refractive index distribution also exhibit optical activity [16]. The effect of the twist defect in such fibers has been studied in recent works [17]. It has been pointed out that by changing the magnitude of the twist defect one can control the value of the average orbital angular momentum of the outcoming beam. However, those studies were limited to the case of long-period fiber gratings. Meanwhile, the existence of defect-localized modes is possible only in Bragg-type fibers, in which the spatial period of the lattice is comparable with the wavelength.

*c.alexeyev@yandex.ua

In this paper we propose a principle of creating the structures that are able to nestle a topologically charged defect mode. According to this principle, the defect mode with a topological charge may be excited at the boundary of two topologically active media each operating in the Bragg regime. Here a topologically active medium is defined as a medium that possesses the ability to change the topological charge of the incoming field. We illustrate this principle at the example of the exactly solvable problem of a multihelicoidal Bragg fiber with a twist defect. To this end we study the influence of the twist defect in such fibers on the transmission of optical vortices (OVs) and Gaussian beams (GBs). We show that the transmission coefficient for the GB demonstrates band-gap behavior. The presence of the twist defect results in a sharp transmission peak within the transmission gap. In the reflected field the incoming GB is transformed into the OV, whose charge is determined by the topological charge imprinted into the chiral fiber lattice. We show that such peculiarities of the reflection and transmission characteristics arise due to the presence of a localized defect mode. We study the spatial structure of this mode and show that its topological charge coincides with the charge imprinted into the lattice.

II. COUPLED MODES OF BRAGG MULTIHELICOIDAL FIBERS

The refractive index distribution of a defectless MHF is given by [18]

$$n^2(r,\varphi) \approx n_{\rm co}^2[1-2\Delta f(r)] + 2\Delta\delta f_r' r\cos[l(\varphi-\alpha)], \quad (1)$$

where $\alpha = qz$ is the rotation angle of the cross section with coordinate z, Δ is the height of the profile f, $\delta \ll 1$ is the dimensionless parameter of the cross section's deformation, $n_{\rm co}$ is the core's refractive index, $q = 2\pi/H$ is the lattice vector of the helical grating, H is the pitch of the grating, and (r,φ,z) are the cylindrical-polar coordinates. The twist defect is introduced in the standard way (see Fig. 1). Since the greatest effect is obtained in case the defect is located in the middle of the sample [9,10,17] we restrict our further considerations just to this limiting case. In the presence of such a twist defect rotation angle α becomes

$$\alpha = \begin{cases} qz, & z<0 \\ qz+\theta, & z>0 \end{cases}, \quad (2)$$

where θ is the angle of rotational shift at the defect.

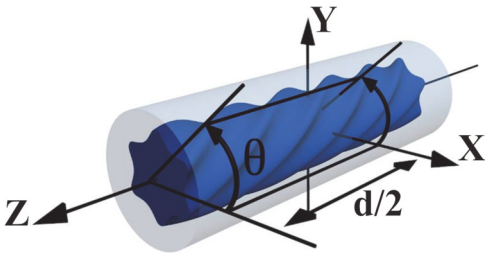

FIG. 1. Geometry of the model of a multihelicoidal fiber with a twist defect. A MHF of length d (here with a hexagonal type of symmetry $\ell = 6$) is cut in the middle across the XY plane. Then its marked half is rotated through an angle θ with respect to the other part.

For an infinite Bragg MHF it proves sufficient to use, for the mode description, the scalar approximation waveguide equation:

$$\nabla^2\mathbf{E}_t + k^2n^2\mathbf{E}_t = 0, \quad (3)$$

where $\mathbf{E}_t$ is the transverse electric field, k is the wave number in vacuum, ∇^2 is the Laplace operator, and the refractive index is given by Eq. (1). Under the change of variables $\tilde r = r, \tilde z = z, \tilde\varphi = \varphi - qz$, one restores the translational invariance in $\tilde z$ of Eq. (3), which upon substitution, $\mathbf{E}_t = \mathbf{e}_t(\tilde r,\tilde\varphi)\exp(i\beta\tilde z)$, where β is some propagation constant, becomes

$$\left\{\frac{\partial^2}{\partial\tilde r^2} + \frac{1}{\tilde r}\frac{\partial}{\partial\tilde r} + \frac{1}{\tilde r^2}\frac{\partial^2}{\partial\tilde\varphi^2} + \left(i\bar\beta - q\frac{\partial}{\partial\tilde\varphi}\right)^2 + k^2n^2(\tilde r,\tilde\varphi)\right\} \times \mathbf{e}_t(\tilde r,\tilde\varphi) = 0. \quad (4)$$

Treating the φ-periodic part of the refractive index as perturbation one can obtain for the spectrum $\bar\beta_m$ of zero-approximation equation

$$\left\{\frac{\partial^2}{\partial\tilde r^2} + \frac{1}{\tilde r}\frac{\partial}{\partial\tilde r} + \frac{1}{\tilde r^2}\frac{\partial^2}{\partial\tilde\varphi^2} + \left(i\bar\beta - q\frac{\partial}{\partial\tilde\varphi}\right)^2 + k^2\tilde n^2(\tilde r,\tilde\varphi)\right\} \times \tilde{\mathbf{e}}_t(\tilde r,\tilde\varphi) = 0, \quad (5)$$

where $\tilde n^2 = n_{\rm co}^2[1-2\Delta f(r)]$, the following result:

$$\bar\beta = \pm\tilde\beta_m + mq. \quad (6)$$

Here $m = 0, \pm 1\cdots$ and the upper sign relates to forward-propagating fields, whereas the lower sign describes backward-propagating fields. In the basis of linear polarizations $|e\rangle = \mathrm{col}(e_x,e_y)$ the solutions of Eq. (5) can be chosen in the form of circularly polarized OVs:

$$|\sigma,m\rangle = \begin{pmatrix} 1 \\ i\sigma \end{pmatrix}\exp(im\tilde\varphi)F_m(r), \quad (7)$$

where $\sigma = \pm 1$ specifies the sign of polarization, m coincides with the topological charge of the OV, and F_m satisfies $(\frac{\partial^2}{\partial r^2} + \frac{1}{r}\frac{\partial}{\partial r} + k^2\tilde n^2 - \frac{m^2}{r^2} - \tilde\beta_m^2)F_m(r) = 0$. Here $\tilde\beta_m$ is the scalar propagation constant of the ideal fiber's mode with the orbital index m.

On the plane (q,β) zero-approximation spectral curves are given by straight lines, which may intersect at certain q. Figure 2 illustrates such intersection events for spectral curves of the fundamental mode $|1,0\rangle$ and the OVs $|1,\pm m\rangle$. It should be noted that there are two points of intersection with the same lattice parameter q. In the first point (a) the forward-propagating mode $|1,0\rangle$ gets coupled with the backward-propagating mode $|1,m\rangle$. In the point (b) the backward-propagating mode $|1,0\rangle$ couples with forward-propagating mode $|1,-m\rangle$. In such points of accidental degeneracy to allow for φ-periodic perturbation it is necessary to use perturbation theory with degeneracy to study the effect of perturbation on modification of spectral curves. Although there

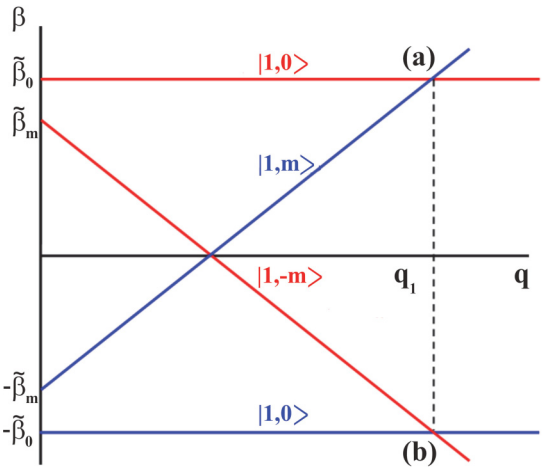

FIG. 2. Zero-approximation spectra of MHF modes vs reciprocal lattice vector q. The type of the mode is indicated at the corresponding curve. Red lines correspond to forward-propagating modes, blue ones to backward-propagating fields.

are also intersections points where copropagating modes may be coupled (not shown in Fig. 2), in the following we focus our attention on coupling between forward- and backward-propagating zero-approximation modes, which corresponds to a Bragg-type coupling. The spectral curves β_m and $\beta_{m'}$ of such oppositely propagating modes intersect at

$$q_i = \frac{\tilde{\beta}_m + \tilde{\beta}_{m'}}{m' - m}, \tag{8}$$

which represents the generalized kinematical Bragg condition for the fields with nonzero topological charges. Near such points one should construct the matrix H_{ij} of the total differential operator on the left of Eq. (4) on the basis of those zero-approximation eigenvectors $|\sigma,m\rangle$ and $|\sigma',m'\rangle$, whose spectral curves intersect at the point given by Eq. (8). This procedure entails obtaining the matrix element $V_{ij} = \langle i|\hat{V}|j\rangle$ of the perturbation operator $\hat{V} = -2k^2 n_{co}^2 \tilde{r}\Delta\delta f'_{\tilde{r}} \cos(l\tilde{\varphi})$. Note that since $\hat{V}$ does not affect the polarization of the state, the polarizations of the coupled eigenvectors are the same; that is, $\sigma = \sigma'$. In this way, the matrix elements can be calculated using the standard definition of the scalar product, $\langle a \mid b\rangle = \iint_S a^* b dS$, where S is the total cross section. Also, due to the specific form of $\hat{V}$ these matrix elements prove to be nonzero if the following dynamical selection rule is fulfilled:

$$|m - m'| = l. \tag{9}$$

Otherwise the fields do not couple in the intersection points.

If one of the coupled fields is the fundamental mode with $m = 0$, the condition Eq. (9) yields $|m'| = l$; that is, the fundamental mode can be coupled to the counterpropagating OV of the same polarization and with topological charge $\pm l$. Then the only nonzero matrix elements generated by perturbation $\hat{V}$ are

$$V_{12} = V_{21} = \langle\sigma,0|\hat{V}|\sigma,l\rangle = -\frac{k^2 n_{co}^2 \Delta\delta}{N_0 N_l} \equiv A. \tag{10}$$

Here we assume a step-index fiber; the normalization factors are $N_i^2 = \int_0^\infty x F_i^2(x) dx$. For this situation the coordinates of intersection points on the plane (q,β) are $a(q_1,\tilde{\beta}_0)$ and $b(q_1, -\tilde{\beta}_0)$, where $q_1 = (\tilde{\beta}_0 + \tilde{\beta}_l)/l$. The matrix of the operator on the left of Eq. (4) built on the basis of eigenvectors $|1,0\rangle$ and $|1,l\rangle$ has the form

$$H = \begin{pmatrix} \tilde{\beta}_0^2 - \beta^2 & A \\ A & \tilde{\beta}_l^2 - (\beta - lq)^2 \end{pmatrix}. \tag{11}$$

This matrix enables one to determine the structure of hybrid modes and their spectrum β near the intersection point (a) through solving the eigenvalue equation $H\mathbf{x} = 0$. The eigenvector $\mathbf{x} = \mathrm{col}(x_1,x_2)$ defines the hybrid mode $|\Psi\rangle$ as $|\Psi\rangle = x_1|1,0\rangle + x_2|1,l\rangle$. Near the point (b) one should invert in Eq. (11) the sign of l, as well as in the expression for $|\Psi\rangle$.

It is advantageous to introduce near these intersection points the detunings $\delta^{a,b}$ and ε as

$$\beta = \mp\tilde{\beta}_0 + \delta^{a,b}, \quad q = q_1 + \varepsilon, \tag{12}$$

which reduces the eigenvector problem to

$$\begin{bmatrix} \mp 2\tilde{\beta}_0\delta^{a,b} & A \\ A & \pm 2\tilde{\beta}_l(\delta^{a,b} \mp l\varepsilon) \end{bmatrix} \mathbf{x}_{a,b} = 0, \tag{13}$$

where the upper sign corresponds to the point (a). The spectrum corrections

$$\delta^a_{1,2} = 0.5(l\varepsilon \pm R), \quad \delta^b_{1,2} = 0.5(-l\varepsilon \pm R), \tag{14}$$

where $R = (l^2\varepsilon^2 - Q^2)^{1/2}$ and $Q^2 \approx A^2/\tilde{\beta}_0^2$, describe repulsion of spectral curves, which leads to the appearance of spectral gaps of width Q/l in the q domain. Note that both gaps have identical position and width. The coupled modes near the upper intersection point (a) look like

$$\begin{aligned} |\psi_{1a}\rangle &= \{p_1|1,0\rangle + p_2|1,l\rangle e^{-iqlz}\}\exp(i\beta_+ z), \\ |\psi_{2a}\rangle &= \{p_2|1,0\rangle + p_1|1,l\rangle e^{-iqlz}\}\exp(i\beta_- z), \end{aligned} \tag{15}$$

where $\beta_\pm = (lq - lq_1 \pm R)/2$ and $p_{1,2} = (1 \mp R/l\varepsilon)^{1/2}/\sqrt{2}$. Note that these modes are essentially the combinations of forward-propagating fundamental mode $|1,0\rangle$ and backward-propagating OV $|1,l\rangle$, as is implied by Fig. 2. Analogously, the expressions for coupled modes near the lower intersection point (b) are

$$\begin{aligned} |\psi_{1b}\rangle &= \{p_2|1,0\rangle + p_1|1,-l\rangle e^{ilqz}\}\exp(i\beta_- z), \\ |\psi_{2b}\rangle &= \{p_1|1,0\rangle + p_2|1,-l\rangle e^{ilqz}\}\exp(i\beta_+ z). \end{aligned} \tag{16}$$

These hybrid modes are also the superposition of oppositely propagating fields. These results could be also obtained by the standard coupled mode theory. It should be emphasized that along with the coupled modes, Eqs. (15) and (16), there are also two nonhybridized OVs: the forward-propagating OV $|1,l\rangle$ and backward-propagating OV $|1,-l\rangle$. These six fields constitute the complete set of modes for studying transmission of the GB through MHFs with twist defects.

III. TRANSMISSION CHARACTERISTICS AND CROSSOVER

Knowing the set of modes of an infinite regular MHF enables one to study the transmission of GBs through a finite-length MHF with a twist defect. The expressions for modes in the rotated section of the fiber are obtained by the following transformation of the basis fields $|\sigma,l\rangle$:

$$|\sigma,l\rangle \rightarrow |\sigma,l\rangle \exp\left[i(l+\sigma)\theta\right] \equiv |\sigma,l\rangle'. \tag{17}$$

This phase transformation is formally similar to the appearance of the Pancharatnam-Berry phase for the light with both spin (σ) and orbital (l) angular momentum, which is currently in the focus of research in connection with its manifestation in various physical processes [19]. However, the phase transformation, Eq. (17), is only formal and emerges due to coordinate frame rotation at the boundary, which we introduce in the expressions for modes to allow for the twist defect. Since at the boundary the field's polarization and the amplitude of the electric field do not change, this phase transformation does not correspond to any evolution of the field's state, which could be the reason for the appearance of the actual Pancharatnam-Berry phase. Naturally, no spin-dependent effects of the kind reported in [19] can be present in the system in the chosen scalar approximation, where polarization degrees of freedom are decoupled from the orbital ones.

To study the transmission of the incident GB through this system we assume that near the input end such a beam can be represented by the $|1,0\rangle$ field. Near the input end the field is given by the following superposition of incident and reflected fields:

$$|\Phi_1(z \leqslant -d/2)\rangle = |1,0\rangle e^{ikz} + (R_1|1,0\rangle + R_2|1,l\rangle + R_3|1,-l\rangle)e^{-ikz}. \tag{18}$$

Within the first section of the fiber the field can be represented as

$$|\Phi_2(-d/2 < z < 0)\rangle = T_1|\psi_{1a}\rangle + T_2|\psi_{2a}\rangle + T_3|\psi_{1b}\rangle + T_4|\psi_{2b}\rangle + T_5|1,l\rangle e^{i\tilde{\beta}_l z} + T_6|1,-l\rangle e^{-i\tilde{\beta}_l z}. \tag{19}$$

The field in the twisted section $[|\Phi_3(0 < z < d/2)\rangle]$ is obtained from this equation by making the substitution $|\sigma,l\rangle \rightarrow |\sigma,l\rangle'$ in the corresponding expressions for modes. Also T_i should be changed to T_i'. The transmitted field should read as

$$|\Phi_4(z \geqslant d/2)\rangle = (P_1|1,0\rangle + P_2|1,l\rangle + P_3|1,-l\rangle)e^{ik(z-d/2)}. \tag{20}$$

Here R_i, T_i, T_i', and P_i are the unknown coefficients. The equations in these coefficients are obtained through matching the fields and their derivatives with respect to z at the boundaries $z = 0$ and $z = \pm d/2$. This enables one to obtain reflection and transmission characteristics of the system in question. We will focus our attention on the case where the fiber is excited with the circularly polarized GB. In the following we carry out numerical simulations for the case $l = 4$. Additionally, we set $\theta = \pi/4$, which corresponds to the maximal influence of the defect.

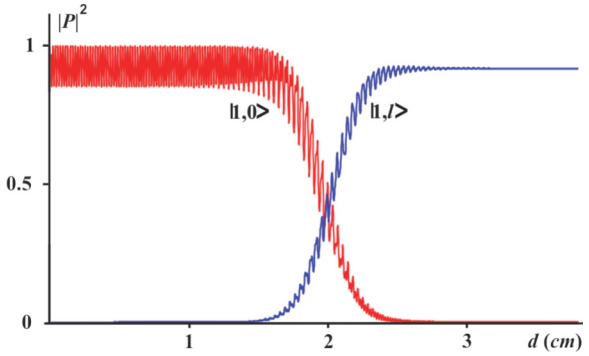

FIG. 3. Crossover event for $l = 4$ fiber with a twist defect; $d_{co} \approx 2\,cm$. The red curve corresponds to the transmission coefficient for the mode $|1,0\rangle$, whereas the blue one shows the reflection curve of the OV $|1,4\rangle$. Fiber parameters: $\theta = \pi/4$, $n_{co} = 1.5$, $\Delta = 5 \times 10^{-3}$, $\delta = 0.05$, $r_0 = 10\lambda_0$, $\lambda_0 = 632.8\,\text{nm}$, and $q = 7.436 \times 10^6\,\text{m}^{-1}$. The fiber is excited with the GB $|1,0\rangle$.

Chiral fibers are known to possess topological activity in the reflected field [20]: If the resonance Bragg condition is met the input GB gets backward scattered into the OV of charge l [18]. Also, a fraction of the Gaussian component is present in the transmitted field. The effectiveness of such conversion essentially depends on the fiber's length. Evidently,

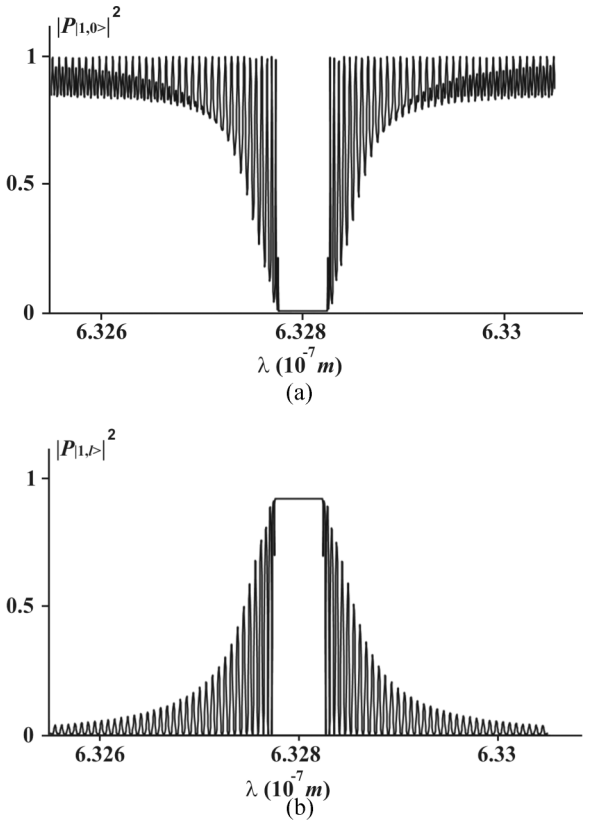

FIG. 4. Transmission coefficient for $|1,0\rangle$ mode (a) and reflection curve for $|1,4\rangle$ OV (b) vs wavelength beyond the crossover length, $d = 2d_{co}$.

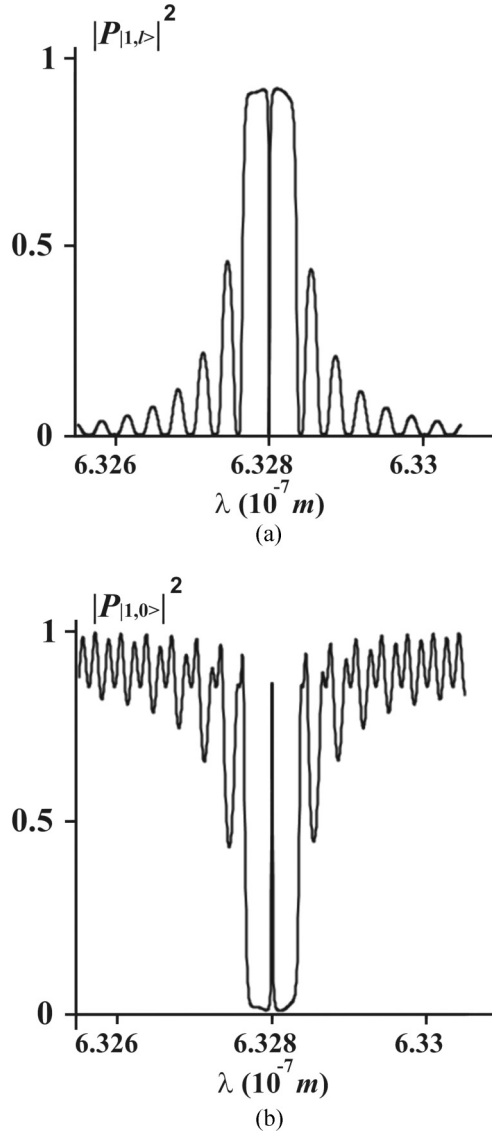

FIG. 5. Transmission coefficient for $|1,0\rangle$ mode (a) and reflection curve for $|1,4\rangle$ OV (b) vs wavelength below the crossover length, $d = 0.4d_{co}$.

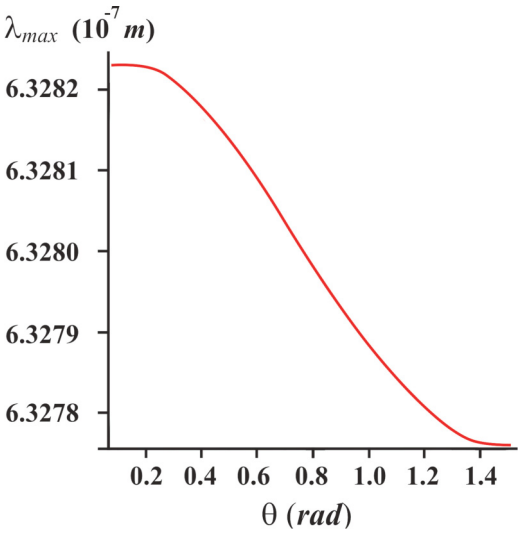

FIG. 6. Shift of the position of the transmission peak within the transmission gap vs defect angle θ below the crossover length, $d = 0.4d_{co}$.

for relatively short fibers the share of the reflected OV should be smaller than the one of the transmitted GB. For long fibers the situation should reverse. Figure 3 shows the transmitted power of the GB and reflected power of $|1,l\rangle$ OV as function of the fiber length d. As is seen, at certain length d_{co}, known as the crossover length, these two curves intersect. This phenomenon of crossover—to the best of our knowledge, first pointed out in [9]—along with the crossover length, plays a rather formal role for defectless MHFs. On the contrary, for MHFs with twist defects this parameter is crucial for the behavior of transmission characteristics. Indeed, at $d > d_{co}$ in the narrow spectral range the transmission coefficient for the $|1,0\rangle$ mode falls to zero [Fig. 4(a)], while the reflection curve for $|1,l\rangle$ OV has the plateau [Fig. 4(b)]. This behavior copies the one for the corresponding transmission (reflection) curves for defectless MHFs [18]. In this way, at $d > d_{co}$ the system converts the incident GB into the reflected OV $|1,l\rangle$ featuring the topological activity. Note that, as has been mentioned in [18], this conversion is not reciprocal: The incident OV $|1,l\rangle$ passes through the system without any changes, so that, in a general sense, there is some orbit-dependent splitting in the system. However, at $d < d_{co}$ in the middle of the spectral gap for transmission of the $|1,0\rangle$ mode a sharp transmission peak appears [Fig. 5(a)]. This event is accompanied by the pronounced dip in the reflection coefficient for the OV $|1,l\rangle$ [Fig. 5(b)]. The position of the transmission peak within the transmission gap depends on the magnitude of θ. As is shown in Fig. 6, for an $l = 4$ MHF with a twist defect the position of the peak shifts from the left margin to the right one if θ changes from zero to $\pi/2$ (maximal influence of defect corresponds to $\theta = \pi/4$). The sharpness of the transmission peak for the $|1,0\rangle$ mode increases exponentially as the fiber's length tends to d_{co}. Figure 7 shows the dependence of $\ln(\Delta B/B)$, where ΔB is the

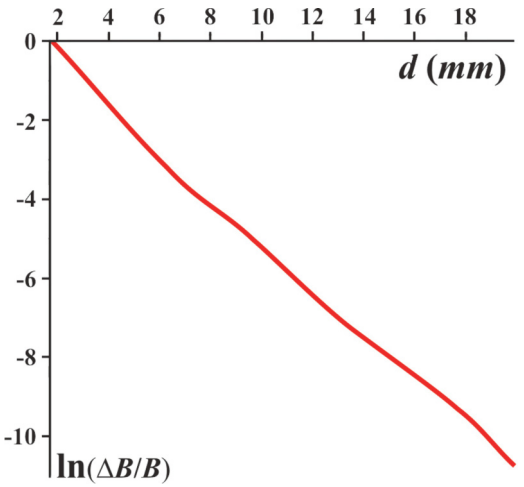

FIG. 7. Logarithm of relative transmission peak width $\Delta B/B$ within the transmission gap for $|1,0\rangle$ mode vs fiber length d. Here B is the peak width at $d \approx 0.1d_{co}$, which approximately coincides with the width of the spectrum gap; $d_{co} \approx 2$ cm, $\theta = \pi/4$.

peak's width and B is the width of the transmission gap for the $|1,0\rangle$ mode, on the fiber's length d. As is seen, at $d = d_{co}$ the initial peak's width decreases approximately 10^5 times. The narrowness of the peak corresponds to a high Q factor of such an effective resonator.

IV. LOCALIZED TOPOLOGICAL STATES

These unusual behaviors of the transmission characteristics below the crossover length are connected with the emergence of defect-localized modes. Since the refractive index, Eq. (1), comprises only a scalar-type perturbation term such modes should be of the same circular polarization as the incident GB. The field within the fiber can be decomposed over the $|1,0\rangle$ fundamental mode and $|1,\pm l\rangle$ OVs as

$$|\Phi_{2,3}\rangle = \sum_{\nu} A_{2,3\nu}|\nu\rangle, \tag{21}$$

where ν specifies the type of the field $|\sigma,l\rangle$. The linear density of energy (that is, energy density integrated over the fiber's cross section) stored in the field is proportional to $|A_{2,3\nu}|^2$. These functions of z comprise rapidly oscillating (on the wavelength scale) interference terms. To exclude such terms one has to carry out averaging over fast spatial oscillations. If the wave vector of the incident GB falls within the spectral gap there emerges localization of energy on the twist defect. Figure 8 shows the distribution of the fast oscillations' averaged energy within the fiber. As is seen, the presence of the defect results in the appearance of three modes localized on the defect: $|1,0\rangle$ and $|1,\pm l\rangle$. Intensity of each of the modes falls off exponentially with the distance z from the defect. An immediate precondition for such exponential behavior lies in the fact that within the spectral gap the mode field, Eqs. (15) and (16), also depend exponentially on the distance from the defect. The two principal defect modes, which give maximal

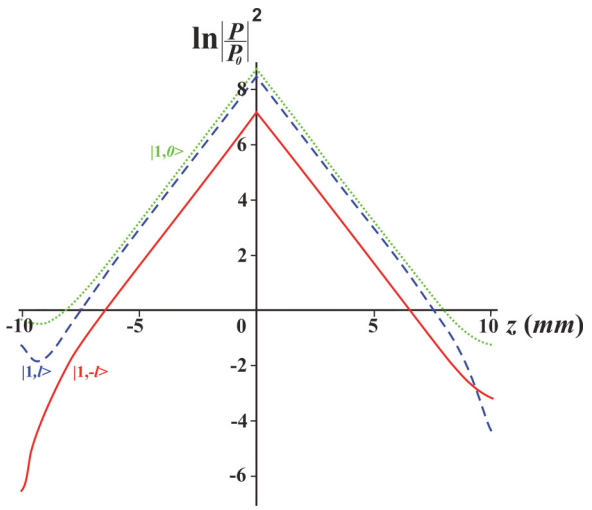

FIG. 8. Logarithm of energy density distribution within the fiber averaged over fast spatial interference oscillations vs position z within the fiber: red solid line is the energy of the OV $|1,-l\rangle$; blue dashed line, energy of the OV $|1,l\rangle$; green dotted line, energy of the fundamental mode $|1,0\rangle$. Here energy density P is normalized to energy density P_0 of the incident GB.

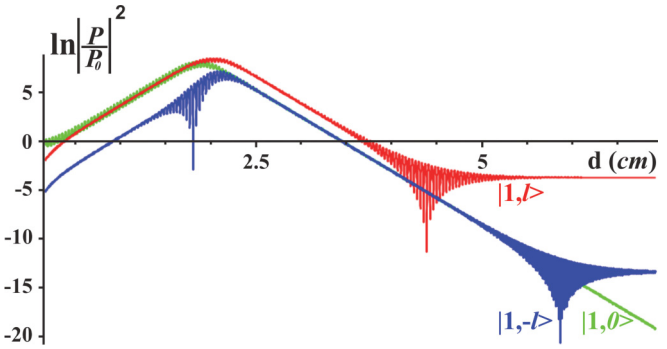

FIG. 9. Logarithm of peak ($z = 0$) relative energy density averaged over fast spatial interference oscillations vs fiber length d for fundamental mode $|1,0\rangle$ (green line); $|1,l\rangle$ OV (red line); $|1,-l\rangle$ OV (blue line).

contributions, are $|1,0\rangle$ and $|1,l\rangle$ OV. In this way, the excitation of a MHF with a twist defect with the GB leads to generation of a localized topological state nested on the defect. It should be noted that since energy density at the input end is unity, the peak energy density strongly exceeds its value in the input beam. This effect of defect mode localization is the strongest at $d = d_{co}$. As d changes, the localization of defect modes becomes less pronounced and, finally, the effect vanishes (see Fig. 9).

There is yet one another property of defect-localized states which has not received due attention in the literature and which might be useful for practical applications. This property concerns the total energy stored in the localized mode. Numerical results show that the value of average energy stored in a sample by the defect mode is sensitive both to the defect angle θ (Fig. 10) and the wavelength of the incident beam (Fig. 11). One can expect, therefore, that by changing the defect parameter one can generate narrow-band pulses of topologically charged light. Such sensitivity of the stored energy to variations of the system's parameters also opens possibilities in controlling the orbital angular momentum (OAM) of light. However, there are drastic differences in

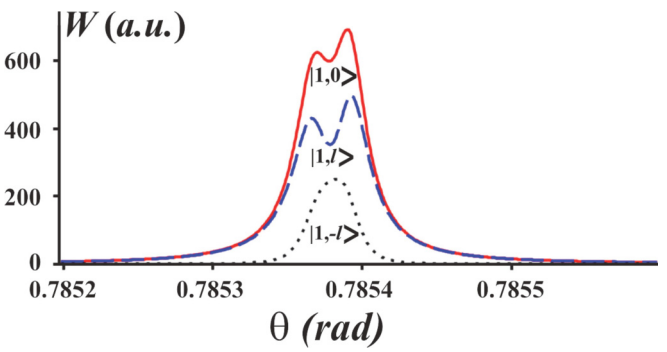

FIG. 10. Average energy density of electromagnetic field (in units of energy density of the incident GB) stored in the mode within the fiber vs θ at the central wavelength $\lambda = \lambda_0$. Red solid line is the energy of the fundamental mode $|1,0\rangle$; blue dashed line, energy of the OV $|1,l\rangle$; black dotted line, energy of the OV $|1,-l\rangle$. Fiber parameters: $\ell = 4$, $d = d_{co} = 0.0202$ m, $n_{co} = 1.5$, $\Delta = 0.005$, and $\delta = 0.05$.

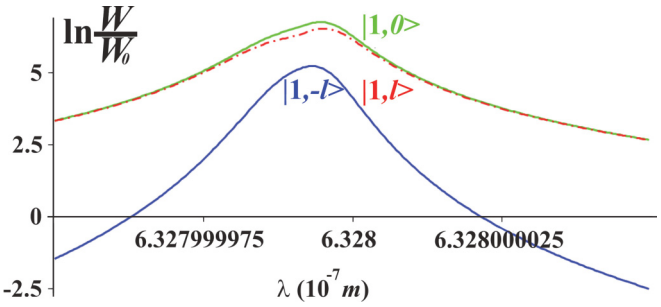

FIG. 11. Relative average energy density of electromagnetic field stored in the mode within the fiber vs wavelength. Blue solid line is the energy of the OV $|1,-l\rangle$; green solid line, energy of the fundamental mode $|1,0\rangle$; red dash-dot line, energy of the OV $|1,l\rangle$. Here W is the energy density; W_0 is the energy density of the incident GB.

the nature of OAM control in Bragg MHFs with defects as compared to such control in long-period chiral fiber gratings [17]. Indeed, in the latter case OAM of the outcoming beam can be continuously changed in a stationary mode by changing the angle of the twist defect. For Bragg MHFs with defects below the crossover length such variation of the twist angle ϑ results only in the shift of the position of the transmission peak within the forbidden area (see Figs. 5 and 6). This shift is not accompanied by the change in the OAM either in transmitted or in reflected fields. One can infer that no OAM control is possible for such a system. However, this is true only for a stationary mode, where the system's parameters are kept intact. Meanwhile, there is a formal possibility that while the OAM of the transmitted (reflected) field is the same for any two twist angles ϑ_1 and ϑ_2 in the stationary mode, it may change in a dynamical process describing this change from ϑ_1 to ϑ_2. Although solving this problem is far beyond the scope of our paper, one can qualitatively assess the possibility of such OAM changing based on the results of the presented stationary treatment.

To this end it is helpful to determine the OAM of the field stored in defect-localized modes. This can be easily done analogously to the method used while obtaining Figs. 10 and 11 if one invokes the ideas of [21]. According to the results of that paper, in the paraxial approximation the time-averaged linear density L_z of the total OAM in the transverse cross section of the beam is connected with the time-averaged linear density W of the energy in the same cross section through

$$\frac{L_z}{W} = \frac{1}{\omega}\frac{\langle\Phi| - i\frac{\partial}{\partial\varphi}|\Phi\rangle}{\langle\Phi\mid\Phi\rangle}, \tag{22}$$

where $|\Phi\rangle$ is the state vector in an arbitrary representation; ω is the frequency. It should be emphasized that whereas Eq. (22) is valid for a field propagating in some direction, the defect-localized modes are formed by counterpropagating fields. In this case one should use the modification of Eq. (22) provided in [22]. Upon averaging over fast spatial oscillations one arrives at the relation analogous to Eq. (22), so that for rough estimates one can still use this expression. After straightforward calculations one can obtain for the desired ratio of OAM to energy stored in the system in study,

$$\frac{\omega L_z}{Wl} = \frac{\int_{-d/2}^{d/2}\{|a_l(z)|^2 - |a_{-l}(z)|^2\}dz}{\int_{-d/2}^{d/2}\{|a_l(z)|^2 + |a_{-l}(z)|^2 + |a_0(z)|^2\}dz}, \tag{23}$$

where $a_{\pm l}(z)$ are the amplitudes of OVs with charges $\pm l$ and $a_0(z)$ is the amplitude of the fundamental mode in the decomposition of the field over this basis.

As it turns out, in some cases this OAM is sensitive to the parameters of the system. Figure 12(a) demonstrates its dependence on the sample's length in the process of its mechanical elongation or any such changing of the length that does not alter the number of periods of the helical grating. Such variations change the lattice parameter q, which in certain regions leads to essential variation of the stored OAM. The reason for such variations is that in the points (a)–(c) the picture of energy density in defect modes is not the same. As is seen from Figs. 12(b) and 12(d), in the points (a) and (c) the energy is mostly concentrated in the defect modes connected with $|1,0\rangle$ and $|1,l\rangle$ modes, which results in relatively larger values of specific OAM. On the contrary, in the point (b) [Fig. 12(c)] the energy of the oppositely charged OV $|1,-l\rangle$ almost equals the one of $|1,l\rangle$ OV, which leads to effective reduction of OAM [cf. the nominator in Eq. (23)]. Although in the stationary process in all these points the system simply converts the incident GB into the reflected OV of the same power, upon transition $a \to b$ and $c \to b$ one can expect irradiation of the extra OAM in both directions. In this way, by changing geometrical parameters it may prove possible to achieve modulation of OAM. It is useful to note that for silica with the coefficient of thermal expansion of $5.5 \times 10^{-7}\,\mathrm{K}^{-1}$ the relative elongation necessary for effective modulation of OAM by varying the temperature is achieved at temperature variations of order 0.03 K. The same effect can be obtained through twisting the fiber at a constant length, which would also modulate the lattice parameter q.

The solved problem opens an alternate field in the study of propagation of electromagnetic waves in topologically active chiral media in the presence of defects. Of immediate interest is studying the formation of defect modes in MHFs with an isotropic spacer, in combination with the twist discontinuity defect, as well as with a pitch jump defect [23]. In general, almost any problem concerned with the defect modes in chiral anisotropic systems can find its analog for topologically active media. Although in the optical range fabrication of the studied system presents a challenge, proof-of-principle experiments can be made in a millimeter-wavelength range. In this connection, it is worth recalling that experiments with an analog of the helical-core fiber, which is the representative of the $\ell = 1$ multihelical fibers, have first been reported just for this wavelength range [24].

The main practical application of band-gap periodic structures with defects is connected with the fact that the existence of the defect mode enables low-threshold lasing [8], which is closely related to the increase of the photon's dwell time on the defect. In our case such defect structures are expected to radiate vortex modes; this property might be utilized while creating in-fiber lasers of a novel type. By corresponding engineering of the defect's geometry one can make such devices suitable for operation with a white light source [25]. In addition, the

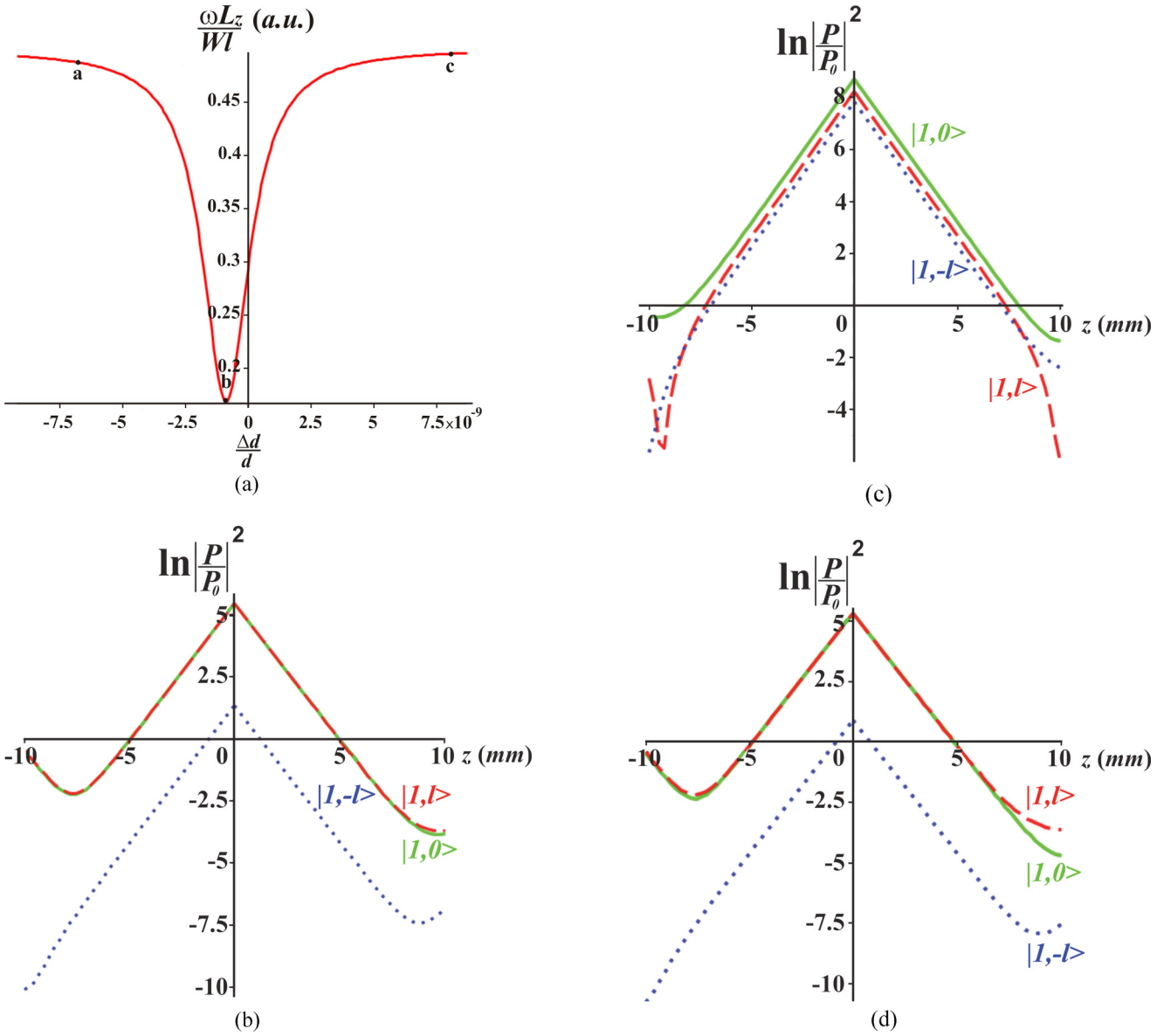

FIG. 12. Panel (a) represents OAM of the defect-localized field (in a. u.) vs relative elongation $\Delta d/d$ of the MHF with the twist defect; $d = 0.01$ m, $l = 6$. Panels (b–d) show logarithm of energy density vs z for points (a–c) marked in (a), respectively. Red dashed line is the energy of the OV $|1,l\rangle$; blue dotted line, energy of the OV $|1,-l\rangle$; green solid line, energy of the fundamental mode $|1,0\rangle$. Lattice parameter at $\delta d = 0$: $q_0 = 7.43 \times 10^6\ \mathrm{m}^{-1}$, $\lambda = 6.32 \times 10^{-7}$.

formulated principle is applicable for generation of vortex beams in the radio-wave range, which might prove useful in connection with recent developments in information transfer via OAM-bearing radio waves [26]. Another application of topologically charged defect modes might be connected with the enhanced nonlinear effects in the vicinity of the defect. Indeed, as follows from our results, energy density at the defect can be greater than the one of the incoming beam by orders. This property is currently of wide interest in connection with the generation of higher harmonics in conventional periodic structures with defects [27].

Based on the obtained result one can put forward a general principle of creating the systems that can nestle topologically charged modes on defects. The first requirement for such systems is the presence of topological activity in bulk samples, that is, the ability to change the topological charge of the incoming field [20]. Secondly, such systems should operate in the Bragg regime to enable contributions of the partial evanescent fields into the defect mode's structure. We believe that under such conditions the system would be able to nestle the topologically charged mode on the defect. The most attractive representatives of topologically active systems, with the example of which one can verify the proposed principle, seem to be the standard q plates [28] and their fiber-array analogs [29].

V. CONCLUSION

In conclusion, we have studied the influence of the twist defect in the multihelicoidal Bragg fibers on the emerging of

localized defect modes. We have shown that if such a fiber with a twist defect is excited with a Gaussian beam this leads to the appearance of the defect-localized topological state, whose topological charge coincides with the order of rotational symmetry of the fiber's refractive index. We have shown that this effect has a pronounced crossover behavior and below the crossover length it is accompanied by the sharp Gaussian mode's transmission peak within the transmission gap. Beyond the crossover length the transmission coefficients for optical vortices and Gaussian modes have a typical band-gap form. We have also put forward a principle of creating the systems that can nestle defect-localized topologically charged modes, according to which such systems have to possess topological activity and operate in the Bragg regime. The candidates for such systems are the q plates and their fiber-array analogs.

ACKNOWLEDGMENT

C.N.A., B.P.L., and M.A.Y. acknowledge the support of the Russian Foundation for Basic Research (RFBR) (Grant No. 16-07-00759).

[1] P. W. Anderson, Absence of diffusion in certain random lattices, Phys. Rev. **109**, 1492 (1958).

[2] A. D. Lagendijk, B. van Tiggelen, and D. S. Wiersma, Fifty years of Anderson localization, Phys. Today **62**(8), 24 (2009).

[3] E. Yablonovitch, Inhibited Spontaneous Emission in Solid-State Physics and Electronics, Phys. Rev. Lett. **58**, 2059 (1987).

[4] E. Yablonovitch, Photonic band-gap structures, J. Opt. Soc. Am. B **10**, 283 (1993).

[5] J. D. Joannopoulos, S. G. Johnson, J. N. Winn, and R. D. Meade, *Photonic Crystals: Molding the Flow of Light*, 2nd ed. (Princeton University Press, Princeton, NJ, 2008).

[6] H. Li, D. B. Phillips, X. Wang, Y.-L. D. Ho, L. Chen, X. Zhou, J. Zhu, S. Yu, and X. Cai, Orbital angular momentum vertical-cavity surface-emitting lasers, Optica **2**, 547 (2015).

[7] E. Yablonovitch, T. J. Gmitter, R. D. Meade, A. M. Rappe, K. D. Brommer, and J. D. Joannopoulos, Donor and Acceptor Modes in Photonic Band Structures, Phys. Rev. Lett. **67**, 3380 (1991).

[8] H. Hoshi and H. Takezoe, Optical second harmonic generation in ferroelectric liquid crystals with a twist defect, Phys. Lett. A **358**, 242 (2006); H. Hoshi, K. Ishikawa, and H. Takezoe, Optical second harmonic generation enhanced by a twist defect in ferroelectric liquid crystals, Phys. Rev. E **68**, 020701 (2003); F. F. Ren, R. Li, C. Cheng, H. T. Wang, J. R. Qiu, J. H. Si, and K. Hirao, Giant enhancement of second harmonic generation in a finite photonic crystal with a single defect and dual-localized mode, Phys. Rev. B **70**, 245109 (2004); L. M. Zhao and B. Y. Gu, Enhanced second-harmonic generation for multiple wavelengths by defect modes in one-dimensional photonic crystals, Opt. Lett. **31**, 1510 (2006).

[9] V. I. Kopp and A. Z. Genack, Twist Defect in Chiral Photonic Structures, Phys. Rev. Lett. **89**, 033901 (2002).

[10] V. I. Kopp, R. Bose, and A. Z. Genack, Transmission through chiral twist defects in anisotropic periodic structures, Opt. Lett. **28**, 349 (2003).

[11] J. Schmidtke, W. Stille, and H. Finkelmann, Defect Mode Emission of a Dye Doped Cholesteric Polymer Network, Phys. Rev. Lett. **90**, 083902 (2003).

[12] J. Schmidtke and W. Stille, Photonic defect modes in cholesteric liquid crystal films, Eur. Phys. J. E **12**, 553 (2003).

[13] *Twisted Photons: Applications of Light with Orbital Angular Momentum*, edited by J. P. Torres and L. Torner (Wiley, Hoboken, NJ, 2011).

[14] H. De Raedt, A. Lagendijk, and P. de Vries, Transverse Localization of Light, Phys. Rev. Lett. **62**, 47 (1989); V. E. Lobanov, Y. V. Kartashov, V. A. Vysloukh, and L. Torner, Anderson localization of light with topological dislocations, Phys. Rev. A **88**, 053829 (2013).

[15] C. N. Alexeyev and M. A. Yavorsky, Generation and conversion of optical vortices in long-period helical core optical fibers, Phys. Rev. A **78**, 043828 (2008); C. N. Alexeyev, T. A. Fadeyeva, B. P. Lapin, and M. A. Yavorsky, Generation of optical vortices in layered helical waveguides, *ibid.* **83**, 063820 (2011); C. N. Alexeyev, Generation of optical vortices in spun multihelicoidal optical fibers, Appl. Opt. **51**, 6125 (2012); Y. V. Kartashov, V. A. Vysloukh, and L. Torner, Dynamics of topological light states in spiraling structures, Opt. Lett. **38**, 3414 (2013); C. N. Alexeyev, A. N. Alexeyev, B. P. Lapin, G. Milione, and M. A. Yavorsky, Spin-orbit-interaction-induced generation of optical vortices in multihelicoidal fibers, Phys. Rev. A **88**, 063814 (2013).

[16] X. M. Xi, T. Weiss, G. K. L. Wong, F. Biancalana, S. M. Barnett, M. J. Padgett, and P. S. J. Russell, Optical Activity in Twisted Solid-Core Photonic Crystal Fibers, Phys. Rev. Lett. **110**, 143903 (2013); C. N. Alexeyev, B. P. Lapin, G. Milione, and M. A. Yavorsky, Optical activity in multihelicoidal optical fibers, Phys. Rev. A **92**, 033809 (2015).

[17] C. N. Alexeyev, B. P. Lapin, A. V. Volyar, and M. A. Yavorsky, Helical-core fiber analog of a quarter-wave plate for orbital angular momentum, Opt. Lett. **38**, 2277 (2013); C. N. Alexeyev, Y. A. Fridman, B. P. Lapin, and M. A. Yavorsky, Orbital angular momentum control by a multihelicoidal fiber with a twist defect, J. Opt. **15**, 125401 (2013).

[18] C. N. Alexeyev, Narrowband reflective generation of higher-order optical vortices in Bragg spun optical fibers, Appl. Opt. **52**, 433 (2013).

[19] X. Ling, X. Yi, X. Zhou, Y. Liu, W. Shu, H. Luo, and S. Wen, Realization of tunable spin-dependent splitting in intrinsic photonic spin Hall effect, Appl. Phys. Lett. **105**, 151101 (2014); Y. Liu, X. Ling, X. Yi, X. Zhou, S. Chen, Y. Ke, H. Luo, and S. Wen, Photonic spin Hall effect in dielectric metasurfaces with rotational symmetry breaking, Opt. Lett. **40**, 756 (2015).

[20] C. N. Alexeyev, A. N. Alexeyev, T. A. Fadeyeva, B. P. Lapin, and M. A. Yavorsky, Topological activity of layered chiral optical waveguides, J. Opt. **13**, 095701 (2011).

[21] M. V. Berry, Paraxial beams of spinning light, Proc. SPIE **3487**, 6 (1998).

[22] C. N. Alexeyev, M. A. Yavorsky, and V. G. Shvedov, Angular momentum flux of counter-propagating beams, J. Opt. Soc. Am. A **25**, 643 (2008).

[23] G. Chilaya, A. Chanishvili, G. Petriashvili, R. Barberi, G. Cipparrone, A. Mazzulla, M. P. Dc Santo, H. Sellame, and M. A. Matran, Single mode lasing in multilayer sandwiched systems consisting of cholesteric liquid crystals and dye solution, Proc. SPIE **6637**, 66370M (2007).

[24] V. I. Kopp and A. Z. Genack, Double-helix chiral fibers, Opt. Lett. **28**, 1876 (2003).

[25] N. Y. Ha, Y. Ohtsuka, S. M. Jeong, S. Nishimura, G. Suzaki, Y. Takanishi, K. Ishikawa, and H. Takezoe, Fabrication of a simultaneous red–green–blue reflector using single-pitched cholesteric liquid crystals, Nat. Mater. **7**, 43 (2008).

[26] B. Thidé, H. Then, J. Sjöholm, K. Palmer, J. Bergman, T. D. Carozzi, Y. N. Istomin, N. H. Ibragimov, and R. Khamitova, Utilization of Photon Orbital Angular Momentum in the Low-Frequency Radio Domain, Phys. Rev. Lett. **99**, 087701 (2007); F. Tamburini, E. Mari, A. Sponselli, B. Thidé, A. Bianchini, and F. Romanato, Encoding many channels on the same frequency through radio vorticity: first experimental test, New J. Phys. **14**, 033001 (2012).

[27] C.-J. Kim, L. Brown, M. W. Graham, R. Hovden, R. W. Havener, P. L. McEuen, D. A. Muller, and J. Park, Stacking order dependent second harmonic generation and topological defects in h-BN bilayers, Nano Lett. **13**, 5660 (2013); Y. Zhang and Q. Zhu, Investigation of coupled third harmonic generation in one-dimensional defective nonlinear photonic crystals, Opt. Express **15**, 6908 (2007).

[28] L. Marrucci, C. Manzo, and D. Paparo, Optical Spin-to-Orbital Angular Momentum Conversion in Inhomogeneous Anisotropic Media, Phys. Rev. Lett. **96**, 163905 (2006).

[29] C. N. Alexeyev, Circular array of anisotropic fibers: A discrete analog of a q plate, Phys. Rev. A **86**, 063830 (2012); C. N. Alexeyev, A. O. Pogrebnaya, G. Milione, and M. A. Yavorsky, Propagation of light in a circular array of elliptical fibres, J. Opt. **18**, 025602 (2016).